# **PCCP**



PAPER View Article Online



Cite this: DOI: 10.1039/c8cp06581k

# Vibrational predissociation of the phenol-water dimer: a view from the water

Daniel Kwasniewski, D Mitchell Butler + and Hanna Reisler +

The vibrational predissociation (VP) dynamics of the phenol–water (PhOH– $H_2O$ ) dimer were studied by detecting  $H_2O$  fragments and using velocity map imaging (VMI) to infer the internal energy distributions of PhOH cofragments, pair-correlated with selected rotational levels of the  $H_2O$  fragments. Following infrared (IR) laser excitation of the hydrogen-bonded OH stretch fundamental of PhOH (Pathway 1) or the asymmetric OH stretch localized on  $H_2O$  (Pathway 2), dissociation to  $H_2O$  + PhOH was observed.  $H_2O$  fragments were monitored state-selectively by using 2+1 Resonance-Enhanced Multiphoton Ionization (REMPI) combined with time-of-flight mass spectrometry (TOF-MS). VMI of  $H_2O$  in selected rotational levels was used to derive center-of-mass (c.m.) translational energy ( $E_T$ ) distributions. The pair-correlated internal energy distributions of the PhOH cofragments derived *via* Pathway 1 were well described by a statistical prior distribution. On the other hand, the corresponding distributions obtained *via* Pathway 2 show a propensity to populate higher-energy rovibrational levels of PhOH than expected from a statistical distribution and agree better with an energy-gap model. The REMPI spectra of the  $H_2O$  fragments from both pathways could be fit by Boltzmann plots truncated at the maximum allowed energy, with a higher temperature for Pathway 2 than that for Pathway 1. We conclude that the VP dynamics depends on the OH stretch level initially excited.

energetics. 1-19

Received 22nd October 2018, Accepted 27th November 2018

DOI: 10.1039/c8cp06581k

rsc.li/pccp

#### 1. Introduction

Recent advances in biological research have created an immense drive not only to broaden but also to deepen our understanding of the fundamental interactions that govern the behavior of biologically relevant systems. Hydrogen bonds (H-bonds) play a central role in numerous biochemical structures and processes, and thus elucidating their characteristic behavior should be helpful, for example, in protein and enzyme design efforts. However, detailed experimental characterizations of the dynamics of H-bonds are sparse. This is due in large part to difficulties in isolating and studying H-bonded systems that are sufficiently small and amenable to experimental interrogation.

Clusters of small molecules weakly bound to water provide excellent model systems for studying H-bonds at the most fundamental level. Phenol (PhOH) and its derivatives are ubiquitous in biochemical systems, such as the side chain of the amino acid tyrosine, and phenolic compounds play essential roles in electron transport, signaling pathways, and other biological processes. It is therefore not surprising that numerous studies have focused on the phenol-water (PhOH-H<sub>2</sub>O) H-bonded dimer

H<sub>2</sub>O moieties are individually planar, but the planes are mutually nearly perpendicular.

Experimental studies of the PhOH-H<sub>2</sub>O dimer have focused on infrared (IR) and ultraviolet (UV) spectroscopy; energy

in the gas-phase and elucidated its structure, spectroscopy, and

shown in Fig. 1.9 Bond lengths and angles were determined

using microwave spectroscopy. The angle  $\beta$  between the plane

of H<sub>2</sub>O and the H-bond coordinate is 108.7°. The PhOH and

The geometry of PhOH-H<sub>2</sub>O in the ground electronic state is

on infrared (IR) and ultraviolet (UV) spectroscopy; energy transfer following vibrational excitation; and determination of the H-bond dissociation energy ( $D_0$ ). Courty *et al.*<sup>4</sup> and Braun *et al.*<sup>2</sup> independently determined  $D_0$  by similar methods. In both studies, thermochemical cycles based on the energies of

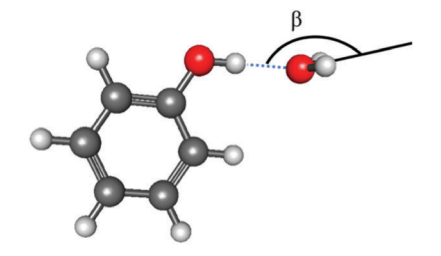


Fig. 1 Structure of the PhOH–H<sub>2</sub>O dimer. The angle  $\beta$  = 108.7° represents the angle between the plane of H<sub>2</sub>O and the H-bond coordinate.<sup>9</sup>

Department of Chemistry, University of Southern California, Los Angeles, California 90089-0482, USA. E-mail: reisler@usc.edu

† Present address: University of Illinois at Chicago College of Medicine, Chicago, Illinois. 60607.

several ground  $(S_0)$  and excited  $(S_1)$  electronic state transitions in bare PhOH and PhOH- $H_2O$  were used.  $D_0$  values of 1960  $\pm$  40 cm<sup>-1</sup> and 1916  $\pm$  30 cm<sup>-1</sup> were determined for  $S_0$  by Courty *et al.*<sup>4</sup> and Braun *et al.*, respectively. Miyazaki *et al.*<sup>13</sup> examined the vibrational dynamics of the PhOH- $H_2O$  dimer and its deuterated analog by using time-resolved IR-UV picosecond pump-probe spectroscopy; they inferred the mechanisms and timescales of intramolecular vibrational energy redistribution (IVR) and predissociation of the dimer after excitation of the H-bonded phenol OH(D) stretch vibration.

The only velocity map imaging (VMI) study that examined PhOH– $\rm H_2O$  was reported by Mazzoni *et al.* <sup>11</sup> Using available data on the electronic spectroscopy of PhOH, measurements of the electronic spectrum of PhOH– $\rm H_2O$ , and photoelectron images of the ionized dimer, these investigators obtained a  $D_0$  value for  $\rm S_0$  that was in good agreement with previous determinations. <sup>2,4</sup> They also attempted to obtain the translational energy distribution of the PhOH fragment ions produced by two-photon two-color ionization of PhOH– $\rm H_2O$ , but due to energy and momentum conservation, the ions velocities were too low to allow a detailed study. Several studies from our group have employed VMI to investigate the vibrational predissociation (VP) dynamics of H-bonded dimers, as well as to derive the predissociation dynamics and accurate  $D_0$  values.

To date, direct interrogation of the H2O fragment in the VP of PhOH-H<sub>2</sub>O has not been reported. This is largely due to predissociation in the upper electronic state used for stateselected 2+1 Resonance Enhanced Multiphoton Ionization (REMPI) detection of the H<sub>2</sub>O fragment and spectral congestion of the rovibronic transitions.<sup>35</sup> In this paper, we report the first study of the energetics and VP dynamics of the PhOH-H2O dimer obtained by examining the H2O fragment. VMI was exploited to obtain complementary information on the PhOH cofragment. Our goal was to elucidate and characterize more completely the H-bond predissociation dynamics of PhOH-H<sub>2</sub>O upon excitation of the two different OH stretch vibrations: the H-bonded OH stretch fundamental of PhOH and the asymmetric OH stretch localized on H2O. The dynamical information derived from the experiments described herein provides fundamental insights into the H-bonding interactions in the PhOH-H<sub>2</sub>O dimer.

# 2. Experimental details

VP of the PhOH–H<sub>2</sub>O dimer generated in a pulsed supersonic molecular beam was studied following IR laser excitation of either the H-bonded OH stretch fundamental of PhOH or the asymmetric OH stretch of H<sub>2</sub>O. Three experimental methods were utilized in the data collection: (1) time-of-flight mass spectrometry (TOF-MS) combined with 2+1 REMPI for spectroscopic investigations of H<sub>2</sub>O fragments; (2) TOF-MS combined with 1+1 REMPI for spectroscopic investigations of the PhOH–H<sub>2</sub>O dimer; and (3) VMI for deriving internal energy distributions of the PhOH cofragment (undetected fragment) and estimating  $D_0$  for PhOH–H<sub>2</sub>O  $\rightarrow$  PhOH + H<sub>2</sub>O.

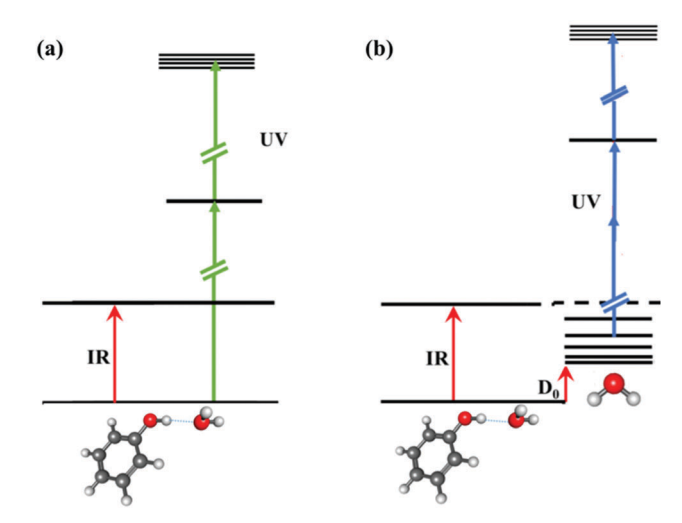


Fig. 2 Experimental scheme for the VP of PhOH $-H_2O$ . IR radiation excites one of the OH-stretch fundamental vibrations of PhOH $-H_2O$ . (a) The dimer is detected by 1+1 REMPI via its S<sub>1</sub> state. (b)  $H_2O$  fragments in the ground vibrational state are detected by 2+1 REMPI via the  $\tilde{C}$   $^1B_1(000)$  state.

Fig. 2 depicts the laser excitation and detection scheme. Upon excitation of the OH-stretch fundamental of the PhOH or  $H_2O$  moiety, energy couples to the H-bond dissociation coordinate and VP ensues. The excess energy is distributed among the center-of-mass (c.m.) translational energy, the rotational levels of  $H_2O$ , and the rovibrational levels of PhOH.

The experimental procedures are similar to those used in previous H-bonded cluster studies.  $^{20-26,32}$  PhOH-H<sub>2</sub>O was generated in the pulsed molecular beam by bubbling He gas (Gilmore, 99.9999%) at 2 atm through 10 mL of liquid water and passing the mixture over 200 mg of solid phenol (Sigma-Aldrich, 99.5%) at room temperature (vapor pressure 0.4 Torr). PhOH was shielded from light to avoid sample degradation. The cluster sample was then expanded through a 0.5 mm orifice of a pulsed piezoelectric valve ( $\sim$ 200 µs opening time) operating at 10 Hz. Expansion conditions (H<sub>2</sub>O and PhOH concentration, and He backing pressure) were optimized to maximize the signal of the PhOH-H<sub>2</sub>O dimer and minimize the concentration of higher order phenol–water clusters. The skimmed molecular beam was intersected at right angles by two counter-propagating laser beams in the interaction region.

IR radiation [1.5 mJ per pulse,  $\sim 0.4~\rm cm^{-1}$  linewidth, focused by a 20 cm focal length (f.l.) lens] excited the H-bonded OH stretch of phenol or the asymmetric OH stretch localized on  $\rm H_2O$  in PhOH– $\rm H_2O$  at 3522 cm<sup>-1</sup> and 3744 cm<sup>-1</sup>, respectively. IR radiation was generated by an optical parametric oscillator/amplifier (OPO/OPA) system (LaserVision), pumped by radiation from a seeded Nd:YAG laser (Continuum Precision II 8000). The IR frequency was calibrated using the photoacoustic spectrum of gaseous NH<sub>3</sub>.  $^{36}$ 

UV radiation for the detection of  $\rm H_2O$  at 80 353–80 808 cm<sup>-1</sup> was generated by frequency-doubling (Inrad Autotracker III) the output of the dye laser (Continuum ND 6000, Coumarin 500) pumped by a Nd:YAG laser (Continuum Surelite); the spectra were frequency calibrated by the known 2+1 REMPI spectrum of  $\rm H_2O.^{35}$  Tightly focused UV radiation ( $\sim$ 0.2 mJ per pulse, lens

f.l. = 20 cm; 0.4 cm<sup>-1</sup> linewidth) ionized state-selected H<sub>2</sub>O fragments while scanning through the  $\tilde{C}$   $^{1}B_{1}(000) \leftarrow \tilde{X}$   $^{1}A_{1}(000)$ transition using 2+1 REMPI. The H<sub>2</sub>O REMPI spectra were simulated using the PGOPHER program<sup>37</sup> with rotational constants from Yang et al.35 From the rotational temperature of background H<sub>2</sub>O monomers in the molecular beam, we estimated the dimer temperature at 25  $\pm$  10 K.

UV radiation for the detection of PhOH-H<sub>2</sub>O at 35 998 cm<sup>-1</sup> was generated by frequency doubling the output of the dye laser (Coumarin 540). The PhOH-H<sub>2</sub>O spectrum was frequency calibrated using published phenol-water cluster spectra at 35 995-36 400 cm<sup>-1</sup>. <sup>12</sup> Unfocused UV radiation (0.3 mJ per pulse, 0.4 cm<sup>-1</sup> linewidth) ionized the PhOH-H<sub>2</sub>O dimer by 1+1 REMPI while scanning through the  $S_1 \leftarrow S_0$  band of the dimer. Spectra were collected by alternating "IR ON" and "IR OFF" conditions at each frequency. In "IR ON," the IR laser was fired 65 ns before the UV laser, and in "IR OFF" the IR laser was fired 2 us after the UV laser. The UV laser conditions for each experiment were varied to optimize the signal-to-noise ratio. Laser timings were adjusted by using delay generators (Stanford, DG535) controlled through a GPIB interface (National Instruments).

The VMI arrangement has been described previously. 20-26,32 Briefly, the apparatus consists of a four-electrode ion acceleration assembly, a 60 cm field-free drift tube, and a microchannel plate (MCP) detector coupled to a phosphor screen (Beam Imaging Solutions, Inc.) that is monitored by a charge coupled device (CCD) camera (LaVision, Imager). In VMI mode, two-dimensional projections were collected using an event counting method (DaVis) and reconstructed to three-dimensional images using the BASEX method.<sup>38</sup> Speed distributions were obtained by summing over the angular distribution of each radius and were converted to c.m.  $E_{\rm T}$ distributions using momentum conservation, the appropriate Jacobian,<sup>39</sup> and calibration constants obtained from previous experiments.<sup>23</sup> The angular distributions were all isotropic.

## 3. Results and discussion

## 3.1 IR depletion spectrum

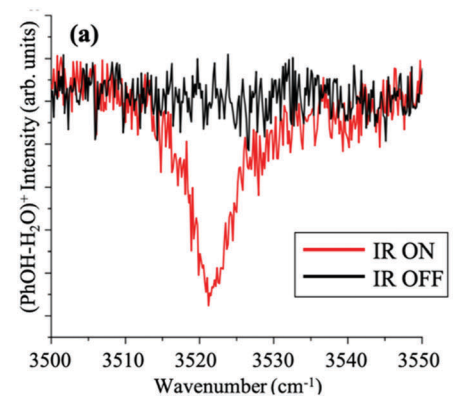
The H-bonded and asymmetric OH stretch fundamental transitions of the PhOH-H<sub>2</sub>O dimer have previously been assigned and

characterized in the gas phase. 5,6,12,16,17,19,40 In this study. IR depletion spectra were obtained by scanning the frequency of the IR laser while monitoring the vibrationless ground state of PhOH- $H_2O$  by REMPI via the  $S_1 \leftarrow S_0$  transition. The position and shape of the dimer peaks agree with the previously reported depletion spectra. Fig. 3 shows the depletion spectra of two different OH stretch transitions of PhOH-H2O: the H-bonded OH stretch localized on phenol and the asymmetric OH stretch localized on H<sub>2</sub>O. The observed vibrational band for the H-bonded OH stretch, centered at 3522 cm<sup>-1</sup>, is well isolated from neighboring OH stretching bands of higher order clusters such as PhOH-(H2O)2  $(3505 \text{ cm}^{-1} \text{ and } 3550 \text{ cm}^{-1})^{19} \text{ and } (H_2O)_3 (3536 \text{ cm}^{-1})^{.22} \text{ The}$ observed vibrational band of the corresponding OH stretch of the H<sub>2</sub>O moiety, centered at 3744 cm<sup>-1</sup>, is located between the closelying free OH stretch vibrations of PhOH-(H2O)2 and (H2O)2 at 3725 cm<sup>-1</sup> and 3729 cm<sup>-1</sup>, respectively, and the  $v_3$  asymmetric stretch of the H<sub>2</sub>O monomer at 3755 cm<sup>-1</sup>. <sup>41</sup> The OH asymmetric stretch localized on H2O of the dimer will be referred to henceforth as the free OH stretch to note that the H atoms do not form hydrogen bonds. The symmetric stretch transition of H<sub>2</sub>O in PhOH-H<sub>2</sub>O was also observed in the gas phase but was found to be very weak. 6,12,17,19

High backing pressure and high H2O concentration can result in the formation of larger clusters; therefore, we optimized the expansion conditions to minimize the formation of larger clusters, as described in Section 2. The temperature of the molecular beam was adjusted to maximize the concentration of dimers. It is essential to ensure that the H2O fragments are produced following one-photon absorption by PhOH-H<sub>2</sub>O. To achieve this, great care was taken to minimize multiphoton absorption. This was achieved by reducing the IR laser fluence and slightly defocusing the radiation passing through the 20 cm IR lens. Decreasing the IR fluence lowers the signal-to-noise ratio, and the H2O signal is further reduced due to the large number of accessible fragment monomer states as well as predissociation in the upper state in the H<sub>2</sub>O REMPI scheme.<sup>35</sup>

#### 3.2 REMPI spectroscopy of H<sub>2</sub>O fragments

In the REMPI and VMI measurements of H<sub>2</sub>O fragments, the H-bonded and free OH stretch fundamentals were excited at



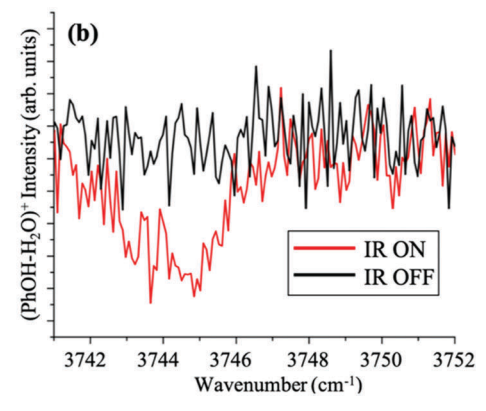


Fig. 3 IR depletion spectra of (a) the H-bonded OH stretch and (b) the asymmetric (free) OH stretch localized on  $H_2O$  of PhOH $_2O$ . The dimer is probed using 1+1 REMPI via the  $S_1 \leftarrow S_0$  transition at 35 998 cm $_2O$ . The IR timing alternates between ON/OFF conditions at each frequency.

This journal is @ the Owner Societies 2018

3522 cm<sup>-1</sup> (Pathway 1) and 3744 cm<sup>-1</sup> (Pathway 2). The excitation energy was (more than) sufficient to induce VP. Fig. 4 displays the "IR ON-IR OFF" 2+1 REMPI spectra of H<sub>2</sub>O fragments following VP. Spectra were obtained by scanning the UV laser frequency in the region of the  $\tilde{C}^{1}B_{1}(000) \leftarrow \tilde{X}^{1}A_{1}(000)$  H<sub>2</sub>O transition. As stated previously, fast predissociation in the C state and spectral congestion limit the state-selective detection of H<sub>2</sub>O. Nevertheless, the 2+1 REMPI spectra were simulated fairly well by rotational temperatures (see Fig. 4). The H<sub>2</sub>O fragment rotational distribution via Pathway 1 was fit best with a temperature of 165  $\pm$  25 K, which corresponds to an average rotational energy of 115  $\pm$  17 cm<sup>-1</sup>. The excess energy in VP in this case is  $1562 \pm 60 \text{ cm}^{-1}$ . In the experiments, rotational levels of the H<sub>2</sub>O fragments up to  $J_{K_a,K_c}^{"} = 7_{1,6}$  (704 cm<sup>-1</sup> energy) could be clearly observed. The REMPI spectrum obtained for Pathway 2 was fit with a rotational temperature of 310  $\pm$  25 K, corresponding to an average rotational energy of 216  $\pm$  17 cm<sup>-1</sup>. The excess energy in this case is  $1784 \pm 60 \text{ cm}^{-1}$ , and rotational levels up to  $J_{K_a,K_c}^{"}=8_{5,3}$  and  $8_{3,6}$  were observed, which have energies of 1255 and 1006 cm<sup>-1</sup>, respectively. The higher H<sub>2</sub>O fragment temperature of Pathway 2 is consistent with these observations. This can also be seen in Fig. 4 by comparing the signal intensities of the  $2_{2,1}$  and  $3_{2,1}$  transitions. The  $2_{2,1}/3_{2,1}$  peak ratio is larger in panel (a) than in (b), as expected from the increase in temperature.

There is not enough excess energy following excitation of the H-bonded OH stretch to populate one quantum of the  $\nu_2$  bending vibration of the  $H_2O$  fragment at 1595 cm $^{-1}$ .<sup>42</sup> However, the excess energy is just high enough to populate this level when exciting the free OH stretch. We searched for evidence of this excitation in the 2+1 REMPI spectrum obtained *via* the  $\tilde{C}$   $^1B_1(000)$   $\leftarrow \tilde{X}$   $^1A_1(010)$   $H_2O$  transition, but the signal-to-noise ratio was far too low to obtain evidence for this pathway.

#### 3.3 Velocity map imaging of the H<sub>2</sub>O fragment

The isolated rotational transitions of H<sub>2</sub>O (000) fragments used for imaging were:  $J_{K_a,K_c}{}' \leftarrow J_{K_a,K_c}{}'' = 2_{0,2} \leftarrow 3_{2,1}, 2_{0,2} \leftarrow 4_{2,3}$ ,

and  $7_{1,7} \leftarrow 7_{1,6}$ . The energies of the ground electronic state rotational levels of these transitions are 212, 300, and 704 cm<sup>-1</sup>, respectively. The pair-correlated  $E_{\rm T}$  distributions were derived from the images as described in Section 2 using conservation of energy:

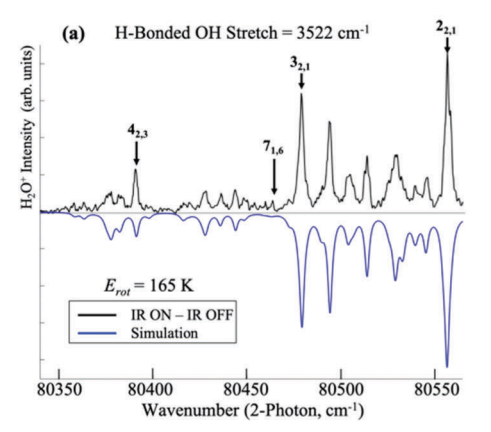
$$hv_{\rm IR} + E_{\rm int}(PhOH-H_2O) = D_0 + E_{\rm T} + E_{\rm rot}(H_2O) + E_{\rm rot,vib}(PhOH)$$
(1)

In eqn (1),  $hv_{\rm IR}$  denotes the excitation energy of one of the OH stretch vibrations;  $E_{\rm int}({\rm PhOH-H_2O})$  is the internal energy of the dimer, estimated at about 20 cm $^{-1}$  based on the temperature of H<sub>2</sub>O monomers in the beam;  $E_{\rm rot}({\rm H_2O})$  is the energy of the monitored rotational level of H<sub>2</sub>O; and  $E_{\rm rot,vib}({\rm PhOH})$  is the rovibrational energy of the PhOH cofragment.

The state-specific c.m.  $E_{\rm T}$  distributions encode dynamical information about the VP process and the internal energy distributions of the PhOH cofragments pair-correlated with each monitored  $\rm H_2O$  rotational level. Below we describe separately results obtained following excitation of the PhOH H-bonded OH stretch (Pathway 1) and the  $\rm H_2O$  free OH stretch (Pathway 2).

**3.3.1 Pathway 1.** Fig. 5 displays the c.m.  $E_{\rm T}$  distributions obtained following excitation of the H-bonded OH stretch of the PhOH moiety of PhOH–H<sub>2</sub>O by monitoring several H<sub>2</sub>O  $J_{K_a,K_c}$ " levels. The arrows indicate the maximum allowed translational energies corresponding to  $D_0=1960~{\rm cm}^{-1}$ , the value measured by Courty *et al.* <sup>4</sup> The observed end points of all three images are in good agreement with this value, as well as with those reported by Neusser *et al.*  $(1916\pm30~{\rm cm}^{-1})^2$  and Mazzoni *et al.*  $(1975\pm60~{\rm cm}^{-1})$ . The angular distributions of the images were isotropic, reflecting the fact that the lifetime of the dimer is of the order of tens of picoseconds. <sup>13</sup>

Based on the findings of Miyazaki *et al.* which showed complete IVR prior to dissociation, <sup>13</sup> and considering the high density of rovibrational states in the PhOH cofragment, we did not expect distinct structures in the images. Indeed, the



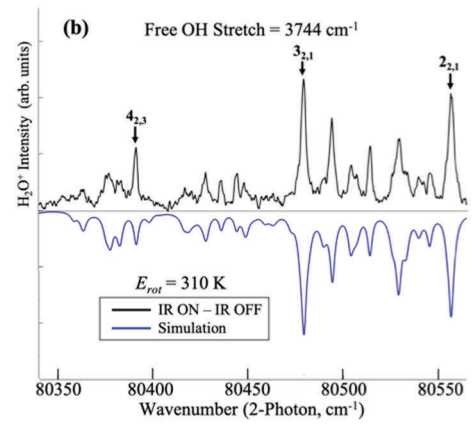


Fig. 4 2+1 REMPI spectra of H<sub>2</sub>O fragments recorded *via* the  $\tilde{C}$  <sup>1</sup>B<sub>1</sub>(000)  $\leftarrow$   $\tilde{X}$  <sup>1</sup>A<sub>1</sub>(000) transition. The *x*-axis gives the wavenumbers required to reach the excited state of H<sub>2</sub>O by 2-photon excitation. The "IR ON-IR OFF" spectrum (top panels, black) was obtained by exciting (a) the H-bonded OH stretch of the PhOH moiety at 3522 cm<sup>-1</sup>, and (b) the free OH stretch of the H<sub>2</sub>O moiety at 3744 cm<sup>-1</sup>. The "IR OFF" spectrum, obtained by recording the background when the IR laser was fired 2  $\mu$ s after the UV laser pulse, was subtracted from the "IR ON" spectrum in which the IR laser was fired 65 ns before the UV laser. The arrows mark the  $J_{K_3,K_2'} \leftarrow J_{K_3,K_2'}$ " transitions monitored in the VMI studies: (a)  $2_{0,2} \leftarrow 3_{2,1}$ ,  $2_{0,2} \leftarrow 4_{2,3}$ , and  $7_{1,7} \leftarrow 7_{1,6}$ , and (b)  $2_{0,2} \leftarrow 3_{2,1}$  and  $2_{0,2} \leftarrow 4_{2,3}$ . Assignments are based on simulated spectra (bottom panels, inverted scale, blue) created by the PGOPHER program.

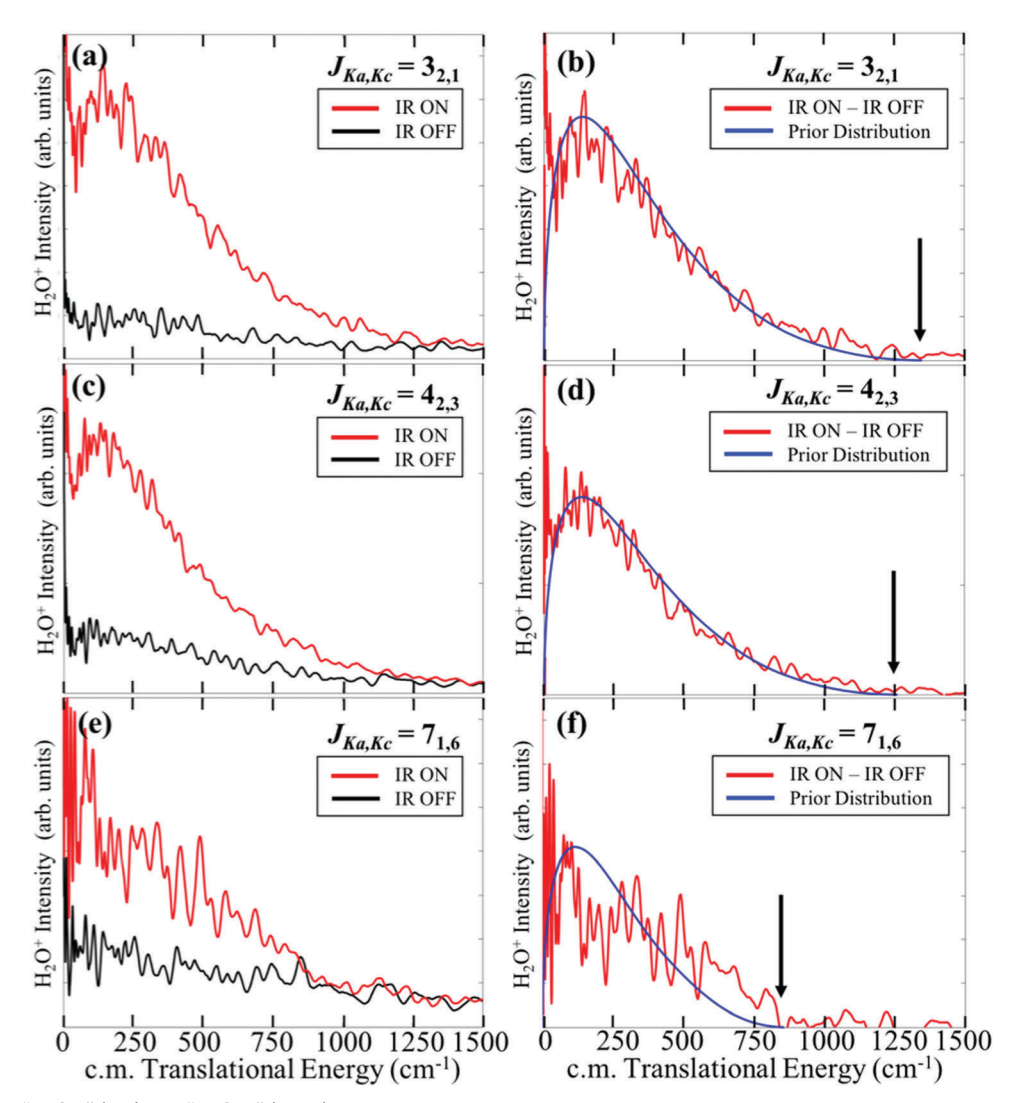


Fig. 5 Left column: "IR ON" (red) and "IR OFF" (black) c.m. translational energy distributions obtained by monitoring state-selected H<sub>2</sub>O fragments in  $J_{K,K}$ " levels: (a)  $3_{2,1}$ , (c)  $4_{2,3}$ , and (e)  $7_{1,6}$  after excitation of the H-bonded OH stretch of PhOH (Pathway 1). Right column: "IR ON-IR OFF" (red) distributions for the same state-selected  $H_2O$  fragments compared with prior distributions (smooth blue lines), (b), (d), (f), respectively. The arrows indicate the maximum allowed translational energies corresponding to  $D_0 = 1960 \text{ cm}^{-1.4}$  This was the value used in the prior calculations as the maximum available energy.

E<sub>T</sub> distributions obtained by monitoring H<sub>2</sub>O fragments with different internal energies show no reproducible structures, and the three images sample the entire range of energetically accessible states. Therefore, the observed  $E_{\mathrm{T}}$  distributions were compared to statistical predictions-specifically, the microcanonical prior distribution of product energies. 43 The prior distributions provide a good first-order picture of statistical behavior because they are based on an unbiased "democratic" model of state populations that imposes no constraints other than energy conservation. The model is based on volumes in phase space for each degree of freedom and involves no dynamics. It has been used successfully, for example, in assessing shapes of distributions in chemical reactions proceeding via a bound intermediates,44 unimolecular reactions,45 and predissociation of dimers, 46 where detailed phase space calculations are unfeasible.

For the case of the PhOH-H<sub>2</sub>O dimer, the relative probability of observing products with translational energy  $E_{\mathrm{T}}$  at energy  $E = E_{\text{avail}} - E_{\text{rot}}(H_2O) \text{ is:}^{43}$ 

$$P^{0}(E_{\mathrm{T}}; E)dE_{\mathrm{T}} \propto \rho_{\mathrm{T}}(E_{\mathrm{T}})\rho_{\mathrm{rot,vib}}(E - E_{\mathrm{T}})dE_{\mathrm{T}},$$
 (2)

where  $\rho_T(E_T)$  is the translational density of states and  $\rho_{\text{rot,vib}}(E-E_T)$ is the rovibrational density of states of the phenol fragment at energy  $E - E_T$ . This simple model gives the pair-correlated microcanonical statistical  $E_{\rm T}$  distributions to which the measured distributions are compared. The calculated distributions for the three monitored rotational levels of H2O are shown as the smooth blue lines in the right panels of Fig. 5 along with the backgroundsubtracted experimental  $E_{\rm T}$  distributions. Neglecting angular momentum conservation should not significantly alter the internal energy distributions of the PhOH cofragment because of its high density of internal states. The model also assumes complete

IVR among levels, disregarding their symmetry. On the other hand, as demonstrated before, the rotational angular momentum of the fragments cannot be too large because there is insufficient anisotropy in the potential energy surface of weakly bound dimers to support a large torque. <sup>28,30,31,47</sup> We therefore limited the rotational angular momentum of the PhOH fragment to 115 cm<sup>-1</sup> (165 K) based on the temperature of the H<sub>2</sub>O fragment obtained experimentally from Pathway 1.

We computed the harmonic vibrational density of states of the PhOH cofragment using the Beyer-Swinehart algorithm with fundamental vibrational levels listed in Roth et al.48 and Schumm et al.49 The algorithm counts all possible harmonic vibrational levels up to the maximum accessible energy (1562 cm<sup>-1</sup>, in our case), and therefore provides a lower limit for the density of vibrational states. Although PhOH is an asymmetric top, for the purpose of our computations, it was sufficient to approximate its geometry as an oblate symmetric top with A = B and Crotational constants of 0.0597 and 0.1885 cm<sup>-1</sup>, respectively. 18 In our implementation, the rotational levels are first counted at discrete energy intervals and folded in before counting the density of vibrational states. The procedure is similar to the one described in ref. 43, which also provides sample computer programs. 43 This procedure gave the dependence of the rovibrational density of states of PhOH,  $\rho_{\text{rot,vib}}$ , on the available energy, as shown in Fig. 6. As expected, the density of rovibrational states is high, and can reach  $1 \times 10^5 \text{ cm}^{-1}$  when the fragment translational energy is low. Finally, we obtained the  $E_{\rm T}$  distributions for the maximum available energies corresponding to each of the monitored  $H_2O$   $J_{K_a,K_c}$ " rotational levels. The pair-correlated calculated  $E_{\rm T}$  distributions are in good agreement with the experimental results, and they support our assertion that the VP of PhOH-H<sub>2</sub>O is statistical-like when the H-bonded OH stretch fundamental is excited.

3.3.2 Pathway 2. To the best of our knowledge this is the first report of the VP dynamics of a mixed dimer of water (HX-H2O) induced by excitation of the free OH stretch vibration of the H<sub>2</sub>O moiety. This study was made possible because in contrast to many other dimers of H2O, the fundamental vibrational transition of the free OH stretch of PhOH-H<sub>2</sub>O was separated from IR transitions of other clusters, as described above. The experiments, however, are more challenging for this pathway because the free OH stretch has a lower oscillator strength than the H-bonded OH transition, and at the same time, the excitation requires using low IR fluences to minimize multiphoton dissociation of larger clusters. As a result, the signals were much smaller than those obtained when exciting the H-bonded OH stretch. Nevertheless, two isolated rotational levels of the H<sub>2</sub>O (000) fragment could be utilized for imaging. Fig. 7 shows the c.m.  $E_{\rm T}$  distributions derived from velocity map images when monitoring the transitions:  $2_{0,2} \leftarrow 3_{2,1}$  and  $2_{0,2} \leftarrow 4_{2,3}$ .

The c.m.  $E_{\rm T}$  distributions for Pathway 2 appear qualitatively different from those observed for Pathway 1. Indeed, paircorrelated prior distributions fail to capture accurately the behavior of the lower- $E_{\rm T}$  region, which corresponds to higher cofragment internal energies; it appears that the populations of the higher rovibrational levels of the PhOH cofragment are

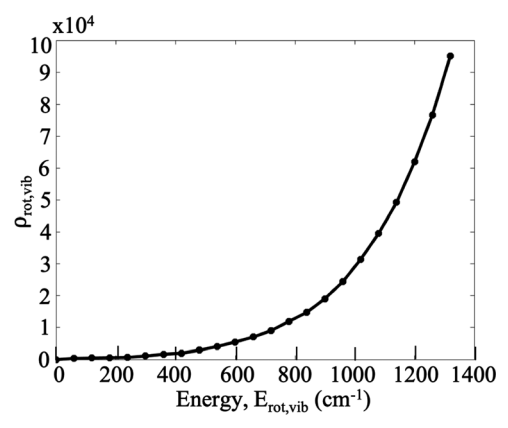


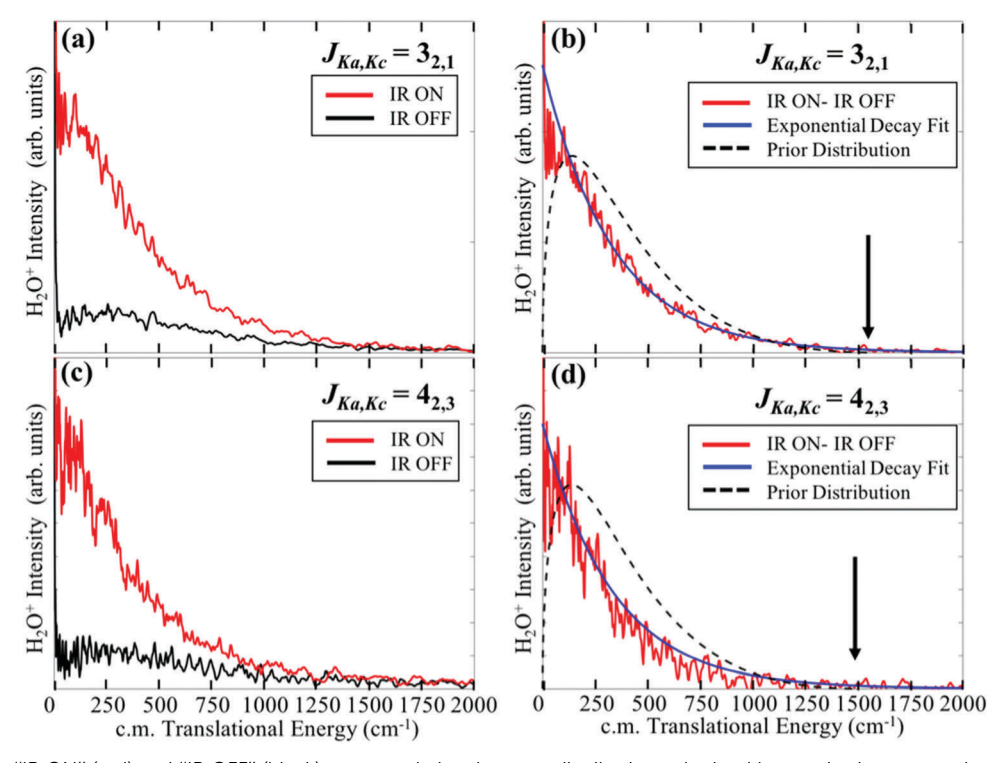
Fig. 6 Calculated rovibrational density of states of the PhOH cofragment as a function of energy. In our experiments the available energies are between 858 and 1350  $cm^{-1}$  for Pathway 1.

underestimated by the prior statistical model. We also compared our results to a model proposed by Ewing,50-52 who used the energy gap law to predict trends in the VP rates of van der Waals dimers of small molecules. In addition to predicting higher VP rates when the energy gap is minimized, Ewing proposed that the "relaxation channel of a vibrationally excited molecule is efficient only when the total change in effective quantum numbers for the process is small."50 In other words, the energy transfer process favors channels with the smallest change in quantum numbers, resulting in a propensity to populate vibration over rotation over translational energy release. To exhibit this propensity, we used an exponentially decaying function to fit the observed  $E_{\rm T}$ distributions. This function included a single fit parameter, C, which was the same for both rotational states shown in Fig. 7:

$$I = e^{-CE_{\rm T}} \tag{3}$$

As seen in Fig. 7, the  $E_{\rm T}$  distributions obtained by VMI are fit better with this function than with the statistical prior distribution.

3.3.3 VP mechanism. The internal energy distributions in fragments of H-bonded dimers following VP range from clearly nonstatistical to statistical-like. When the two subunits of the dimer have a low density of internal states, the internal state distributions often obey propensity rules suggested by Ewing as described briefly above. 50-52 In these cases IVR is incomplete, and the internal state distributions conform to the momentum (or energy) gap law. 28,30,31,34,53,54 Three dimers containing H<sub>2</sub>O (or an isotope thereof) as a subunit, H<sub>2</sub>O-HCl, <sup>20,23</sup> H<sub>2</sub>O-H<sub>2</sub>O, <sup>21,24</sup> and D<sub>2</sub>O-D<sub>2</sub>O,<sup>21</sup> were examined experimentally in detail following excitation of the H-bonded OH stretch. In all three cases the rovibrational energy distribution of the H2O fragment exhibited a clear propensity to populate rovibrational states with high internal energy. Thus, the distributions were found to be nonstatistical obeying eqn (3), similar to those of other dimers with small subunits.34,54 Statistical-like distributions were observed when the H<sub>2</sub>O was part of a larger cluster, such as (H<sub>2</sub>O)<sub>3</sub><sup>22</sup> or HCl-(H<sub>2</sub>O)<sub>3</sub>.<sup>25,26</sup> In these larger clusters the density of states is large and the couplings between the subunits are more efficient; which in turn leads to complete IVR prior to VP.



 $\textbf{Fig. 7} \quad \text{Left column: "IR ON" (red) and "IR OFF" (black) c.m. translational energy distributions obtained by monitoring state-selected $H_2O$ fragments in the property of the propert$  $J_{K_{-}K_{-}}''$  levels: (a)  $3_{2,1}$  and (c)  $4_{2,3}$ , after excitation of the free OH stretch of the  $H_2O$  moiety. Right column: "IR ON–IR OFF" (red) signals for the same stateselected H<sub>2</sub>O fragments fitted with an exponential decaying function (smooth blue solid lines), (b) and (d), respectively. The black dashed lines represent the corresponding prior distributions. The arrows indicate the maximum allowed translational energies corresponding to  $D_0 = 1960 \text{ cm}^{-1.4}$  This was the value used also in the prior calculations and in the decaying function fits.

The VP of PhOH-H<sub>2</sub>O is intermediate between the cases discussed above. Due to the large density of states in PhOH, the dimer may exhibit efficient IVR following excitation of the OH stretch. Miyazaki et al. 13 determined energy transfer rates in bare PhOH and PhOH-H2O by using real time picosecond IR-UV measurements, and found that following excitation of the H-bonded OH stretch of PhOH in PhOH-H<sub>2</sub>O, IVR in the dimer was faster than in bare PhOH. 13 By analyzing the rise and fall curves of several internal levels of the phenol moiety populated by IVR in PhOH-H<sub>2</sub>O and PhOD-D<sub>2</sub>O, they estimated that the IVR lifetime in these dimers is of the order of 10-30 ps, which is shorter by about a factor of 4-5 than the corresponding VP lifetime, estimated at 40 and 100 ps, respectively. 13 They used a model based on anharmonic force fields 13,15 to examine both IVR within the PhOH moiety and the slower energy transfer process involving the intermolecular modes. They also concluded that the experimental VP rates were in reasonable agreement with the ones calculated by RRKM theory.13

The results reported here following excitation of the H-bonded OH stretch of PhOH-H<sub>2</sub>O show statistical energy distributions in the PhOH fragments and therefore reinforce the previous conclusion that complete IVR precedes VP. Achieving complete IVR prior to dissociation is the first step to a statistical internal energy product distribution. Moreover, the test afforded by our results is more stringent because it is based on pair-correlated distributions in the PhOH fragment; this removes the effects of inherent averaging over some degrees of freedom. The H<sub>2</sub>O

fragment rotational distribution, inferred from the REMPI spectrum, is well described by a temperature of 165 K and appears to be statistical as well.

We are not aware of any experiments that investigated the IVR in PhOH-H<sub>2</sub>O following excitation of the free OH stretch of H<sub>2</sub>O. However, we can use for comparison results of IVR in the PhOH dimer following excitation of its H-bonded and free OH stretch vibrations reported by Ebata et al. 55 The authors of that study observed clear site specificity in the IVR lifetimes, which were 5 and 14 ps for the H-bonded and free OH, respectively. The latter value was similar to the IVR lifetime determined for the PhOH monomer. On the other hand, they found that the ensuing VP rate was faster for the free OH excitation than for the H-bonded case, apparently due to incomplete IVR prior to dissociation. Our results, which indicate nonstatistical internal energy distributions in the PhOH cofragments, also suggest incomplete IVR prior to dissociation.

Furthermore, the H<sub>2</sub>O fragment rotational temperature following excitation of the free OH stretch is significantly higher than the corresponding one for the H-bonded OH stretch. Predissociation in the upper electronic state of H<sub>2</sub>O used for the REMPI detection and spectral congestion prevent us from observing a clear propensity to populate high rotational levels of H2O; however, for free OH excitation we detected rotational levels higher than those observed with H-bonded stretch excitation. Also, the increase in rotational temperature—from 165 to 310 K—seems to be larger than what would be expected by the slight increase in

excitation energy for the free OH stretch excitation. Therefore, we suggest that following free OH stretch excitation, VP in PhOH–  $\rm H_2O$  takes place before complete IVR in the PhOH moiety is achieved, and that the rovibrational energy distributions are hotter than expected by statistical considerations.

### 4. Conclusions

Paper

The VP dynamics of the phenol-water (PhOH-H<sub>2</sub>O) dimer were studied by using velocity map imaging of H2O fragments to infer the internal state distributions of PhOH cofragments, pair-correlated with selected rotational levels of the H2O fragment. The parent cluster was excited at two different frequencies corresponding to the H-bonded OH stretch of PhOH (Pathway 1) and the asymmetric stretch (free) OH stretch of H2O (Pathway 2) of the PhOH-H<sub>2</sub>O dimer. We conclude that the predissociation dynamics depends on the OH stretch level initially excited. The results found in this study for Pathway 1, as well as previous results involving PhOH-H<sub>2</sub>O, <sup>13</sup> suggest that complete IVR occurs prior to VP. On the other hand, our results for Pathway 2, inferred from the c.m. E<sub>T</sub> distributions of VMI and the H<sub>2</sub>O 2+1 REMPI spectrum, suggest incomplete IVR prior to VP. Pathway 2 shows a propensity to populate rovibrational levels of PhOH higher in energy than those predicted by a statistical model and is in better agreement with an energy-gap model.

## Conflicts of interest

There are no conflicts to declare.

# Acknowledgements

This work is supported by the National Science Foundation (NSF) Grant No. CHE-1664994.

# References

- I. Bandyopadhyay, H. M. Lee and K. S. Kim, J. Phys. Chem. A, 2005, 109, 1720–1728.
- 2 J. E. Braun, T. Mehnert and H. J. Neusser, *Int. J. Mass Spectrom.*, 2000, **203**, 1–18.
- 3 A. W. Castleman and R. J. Stanley, *J. Chem. Phys.*, 1991, **94**, 7744–7756.
- 4 A. Courty, M. Mons, I. Dimicoli, F. Piuzzi, V. Brenner and P. Millié, *J. Phys. Chem. A*, 1998, **102**, 4890–4898.
- 5 A. Doi and M. Naohiko, J. Chem. Phys., 2008, 129, 154308.
- 6 T. Ebata, N. Mizuochi, T. Watanabe and M. Naohiko, J. Chem. Phys., 1996, 100, 546–550.
- 7 K. Fuke and K. Kaya, Chem. Phys. Lett., 1983, 94, 97-101.
- 8 M. Gerhards and K. Kleinermanns, *J. Chem. Phys.*, 1995, **103**, 7392–7400.
- M. Gerhards, M. Schmitt, K. Kleinermanns and W. Stahl, J. Chem. Phys., 1996, 104, 967–971.
- 10 R. J. Lipert, G. Bermudez and S. D. Colson, *J. Phys. Chem.*, 1988, **92**, 3801–3805.

- 11 F. Mazzoni, M. Pasquini, G. Pietraperzia and M. Becucci, J. Mol. Struct., 2015, 1090, 2–6.
- 12 N. Mikami, Bull. Chem. Soc. Jpn., 1995, 68, 683-694.
- 13 Y. Miyazaki, Y. Inokuchi, T. Ebata and M. Petkovic, *Chem. Phys.*, 2013, **419**, 205–211.
- 14 A. Oikawa, H. Abe, N. Mikami and I. Mitsuo, *J. Phys. Chem.*, 1983, **87**, 5083–5090.
- 15 M. Petković, J. Phys. Chem. A, 2011, 116, 364-371.
- 16 T. Shimamori and A. Fujii, J. Phys. Chem. A, 2015, 119, 1315-1322.
- 17 T. Watanabe, T. Ebata, S. Tanabe and N. Mikami, *J. Chem. Phys.*, 1996, **105**, 408–419.
- 18 G. Berden, W. L. Meerts, M. Schmitt and K. Kleinermanns, J. Chem. Phys., 1996, 104, 972–982.
- 19 S. Tanabe, T. Ebata, A. Fujii and N. Mikami, *Chem. Phys. Lett.*, 1993, **215**, 347–352.
- 20 B. E. Casterline, A. K. Mollner, L. C. Ch'ng and H. Reisler, J. Phys. Chem. A, 2010, 114, 9774-9781.
- 21 L. C. Ch'ng, A. K. Samanta, G. Czakó, J. M. Bowman and H. Reisler, J. Am. Chem. Soc., 2012, 134, 15430–15435.
- 22 L. C. Ch'ng, A. K. Samanta, Y. Wang, J. M. Bowman and H. Reisler, *J. Phys. Chem. A*, 2013, **117**, 7207–7216.
- 23 B. E. Rocher-Casterline, A. K. Mollner, L. C. Ch'ng and H. Reisler, *J. Phys. Chem. A*, 2011, 115, 6903–6909.
- 24 B. E. Rocher-Casterline, L. C. Ch'ng, A. K. Mollner and H. Reisler, *J. Chem. Phys.*, 2011, 134, 211101.
- 25 K. Zuraski, D. Kwasniewski, A. K. Samanta and H. Reisler, *J. Phys. Chem. Lett.*, 2016, 7, 4243–4247.
- 26 K. Zuraski, Q. Wang, D. Kwasniewski, J. M. Bowman and H. Reisler, *J. Chem. Phys.*, 2018, **146**, 204303.
- 27 J. S. Mancini, A. K. Samanta, J. M. Bowman and H. Reisler, J. Phys. Chem. A, 2014, 118, 8402–8410.
- 28 A. J. McCaffery, M. Pritchard and H. Reisler, *J. Phys. Chem.*, 2009, **112**, 412–418.
- 29 A. K. Mollner, B. E. Casterline, L. C. Ch'ng and H. Reisler, J. Phys. Chem. A, 2009, 113, 10174-10183.
- 30 J. A. Parr, G. Li, I. Federov, A. J. McCaffery and H. Reisler, J. Phys. Chem. A, 2007, 111, 7589–7598.
- 31 M. Pritchard, J. Parr, G. Li, H. Reisler and A. J. McCaffery, Phys. Chem. Chem. Phys., 2007, 9, 6241–6252.
- 32 A. K. Samanta, L. C. Ch'ng and H. Reisler, *Chem. Phys. Lett.*, 2013, 575, 1–11.
- 33 A. K. Samanta, G. Czakó, Y. Wang, J. S. Mancini, J. M. Bowman and H. Reisler, *Acc. Chem. Res.*, 2014, 47, 2700–2709.
- 34 A. K. Samanta, Y. Wang, J. S. Mancini, J. M. Bowman and H. Reisler, *Chem. Rev.*, 2016, **116**, 4913–4936.
- 35 C.-H. Yang, G. Sarma, J. J. ter Muelen, D. H. Parker and C. M. Western, *Phys. Chem. Chem. Phys.*, 2010, 12, 13983–13991.
- 36 I. Kleiner, L. R. Brown, G. Tarrago, Q.-L. Kou, N. Picqué, G. Guelachvili, V. Dana and J.-Y. Mandin, J. Mol. Spectrosc., 1999, 193, 46–71.
- 37 C. M. Western, J. Quant. Spectrosc. Radiat. Transfer, 2017, 186, 221–242.
- 38 V. Dribinski, A. Ossadtchi, V. A. Mandelshtam and H. Reisler, *Rev. Sci. Instrum.*, 2002, 73, 2634–2642.
- 39 J. Mooney and P. Kambhampati, *J. Phys. Chem. Lett.*, 2013, **4**, 3316–3318.

**PCCP** 

- 40 T. Ebata, T. Watanabe and N. Mikami, *J. Phys. Chem.*, 1995, **99**, 5761–5764.
- 41 S. Kuma, M. N. Slipchenko, K. E. Kuyanov, T. Momose and A. F. Vilesov, *J. Phys. Chem. A*, 2006, **110**, 10046–10052.
- 42 T. Shimanouchi, Natl. Bur. Stand., 1972, 1, 1-160.
- 43 T. Baer and W. L. Hase, *Unimolecular Reaction Dynamics: Theory and Experiments*, Oxford University Press, Inc., New York, NY, 1996.
- 44 J.-H. Park, H. Lee, K.-C. Kwon, H.-K. Kim, Y.-S. Choi and J.-H. Choi, *J. Chem. Phys.*, 2002, 117, 2017–2028.
- 45 M. Noble, C. X. W. Qian, H. Reisler and C. Wittig, *J. Chem. Phys.*, 1986, **85**, 5763–5773.
- 46 L. M. Yoder, J. R. Parker, K. T. Lorenz and D. W. Chandler, *Chem. Phys. Lett.*, 1999, **302**, 602–608.

- 47 A. J. McCaffery, *Phys. Chem. Chem. Phys.*, 2004, 6, 1637–1657.
- 48 W. Roth, P. Imhof, M. Gerhards, S. Schumm and K. Kleinermanns, *Chem. Phys.*, 2000, 252, 247–256.
- 49 S. Schumm, M. Gerhards, W. Roth, H. Gier and K. Kleinermanns, Chem. Phys. Lett., 1996, 263, 126–132.
- 50 G. E. Ewing, J. Phys. Chem., 1987, 91, 4662.
- 51 G. E. Ewing, J. Chem. Phys., 1980, 72, 2096.
- 52 G. E. Ewing, J. Phys. Chem., 1979, 71, 3143.
- 53 R. E. Miller, Acc. Chem. Res., 1990, 23, 10-16.
- 54 R. E. Miller and L. Oudejans, *Annu. Rev. Phys. Chem.*, 2001, 52, 607–637.
- 55 T. Ebata, M. Kayano, S. Sato and N. Mikami, *J. Phys. Chem. A*, 2001, **105**, 8623–8628.